Overview and Performance of the LOFTID Instrumentation Suite

Gregory T. Swanson[1], Ruth A. Miller[2], Cole D. Kazemba[3], and Hannah S. Alpert[4]
NASA Ames Research Center, Moffett Field, CA 94035

Joseph D. Williams[5]
AMA Inc. at NASA Ames Research Center, Moffett Field, CA 94035

Stephen J. Hughes[6] and Neil Cheatwood[7]
NASA Langley Research Center, Hampton, VA,23681

On November 10, 2022, NASA launched the Low-earth Orbit Flight Test of an Inflatable Decelerator (LOFTID) vehicle as a secondary payload mounted inside the launch vehicle adaptor on an Atlas V out of the Vandenburg Space Force Base (VSFB). The primary payload, Joint Polar Satellite System-2 (JPSS-2), was delivered successfully to a sun synchronous trajectory shortly after launch, at which point the Centaur upper stage performed a burn to de-orbit the system. Once on the desired trajectory to enter the atmosphere the payload adaptor canister was ejected by the payload adapter separation system to expose the packed LOFTID vehicle, then the LOFTID aeroshell, a Hypersonic Inflatable Aerodynamic Decelerator (HIAD), was deployed and inflated as planned. The Centaur pointed the LOFTID vehicle to the desired attitude to enter the atmosphere, spun the assembly to roughly three rpm, and separated the reentry vehicle. The LOFTID vehicle entered the atmosphere over Alaska at >8km/sec and decelerated as designed demonstrating stable flight from hypersonic entry through subsonic parachute deployment. On-board visible light cameras captured the reactions of the heatshield through all phases of flight, and co-located infrared light cameras captured the temperature distribution of the aft side of the heat shield anchored to a distribution of thermocouples on the inflatable structure (IS) in the field of view. Thermocouples were also embedded in the forward side of the aeroshell both in the Flexible Thermal Protection System (FTPS) as well as the IS. Heat Flux Gages and Pressure Transducers measured the heating rate and surface pressure experienced by the rigid nose of the reentry vehicle. Loadcells measured the interface loads between the IS and the rigid centerbody. This paper will discuss many of the key instruments flown on the successful LOFTID technology demonstration mission and will provide some high level results, while pointing to more detailed papers on the post-flight analyses.

[1] LOFTID Instrumentation Lead, Entry Systems and Vehicle Development Branch.
[2] Instrumentation Engineer, Entry Systems and Vehicle Development Branch.
[3] LOFTID Aeroshell Instrumentation Lead, Entry Systems and Vehicle Development Branch.
[4] Aerospace Flight Systems Engineer, Entry Systems and Vehicle Development Branch.
[5] Systems Engineer, Entry Systems and Vehicle Development Branch.
[6] LOFTID Aeroshell Lead, Mechanical Systems Branch.
[7] LOFTID Principal Investigator, Atmospheric Flight and Entry Systems Branch.

I. Nomenclature

α = Schmidt-Boelter gauge coating absorptance
a = temperature-dependent correction coefficient
c = calibration coefficient, W/cm^2 per mV
q = heat flux, W/cm^2
T = temperature, degC
V = voltage, V

Subscripts

cal = *calibration*
THFS = *total heat flux sensor*

II. Introduction

NASA's Hypersonic Inflatable Aerodynamic Decelerator (HIAD) is an enabling technology that facilitates atmospheric entry of heavy payloads to planets such as Earth and Mars using a deployable aeroshell. The deployable nature of the HIAD technology allows it to overcome the size constraints imposed on current rigid aeroshell entry systems. This enables use of larger aeroshells resulting in increased entry system performance (e.g., higher payload mass and/or volume, higher landing altitude at Mars) [1].

On November 10th, 2022, a HIAD technology demonstration mission called Low-Earth Orbit Flight Test of an Inflatable Decelerator (LOFTID), was launched out of Vandenberg Space Force Base as a secondary payload on an Atlas V rocket [2]. After the primary payload was delivered to its orbit, the LOFTID reentry vehicle was inflated, positioned, and then separated to reenter Earth's atmosphere at a velocity of >8 km/s, ultimately splashing down safely in the Pacific Ocean [3]. The flight successfully demonstrated a 6-meter diameter, 70-deg sphere-cone HIAD on a high-energy orbital reentry. This demonstration has provided critical fight data essential to characterize the vehicle performance and support the ongoing effort to further scale the HIAD technology to vehicles of 10-meter diameter or greater. Aeroshells of this scale are applicable to near-term commercial applications and future NASA robotic and human exploration missions.

LOFTID incorporated an extensive instrumentation suite totaling over 150 science measurements. A breakdown of the LOFTID instrumentation suite by vehicle location is shown in Fig. 1. The LOFTID instrumentation suite included thermocouples (TC), total heat flux gages (THFG), and a radiometer to characterize the aeroheating environment and aeroshell thermal response. An Inertial Measurement Unit (IMU), Global Positioning System (GPS), and Flush Air Data System (FADS) were included to allow post-flight reconstruction of the vehicle trajectory and flight dynamics. Fig. 2 shows the TC, HFG, radiometer, and FADS pressure transducer (PT) locations on the LOFTID rigid nose and flank flexible thermal protection system (FTPS). Loadcells were used to measure HIAD structural response during entry, and cameras (in both the visible and infrared wavelengths) were mounted on the aft segment looking at the aeroshell to monitor structural deflection and surface temperature distribution, respectively. A single rearward facing "uplook" camera was included to provide qualitative assessments of the Centaur separation and parachute deployment events, but the spectacular footage captured during the hypersonic entry phase has enabled additional science insights regarding wake characteristics and vehicle dynamics.

The inflation system was instrumented with pressure transducers (torus pressure, manifold pressure, ambient pressure, and tank pressure), Resistance Temperature Detectors (RTDs) to measure tank and gas flow temperatures, a flow meter, and hot film anemometers to determine when the relief valves open and close. Due to an onboard network error, there was no onboard recording of IMU or GPS data, and the majority of the inflation system data was also not recorded [2]. The data from the hot film anemometers was recorded and returned. The analysis of the available inflation system data can be found in Ref. 4.

In addition to the primary instrumentation suite, a new Fiber Optic Sensing System (FOSS) was used to provide global temperature distributions as a technology demonstration. The system provided over 200 thermal measurements creating a thermal map for the backside of the nose Flexible Thermal Protection System. Another pair of FOSS fibers were run along the rigid center structure and measured the temperature response to the vehicle wake environment. The LOFTID instrumentation suite leveraged Agency-wide expertise, with hardware development occurring at Ames Research Center, Langley Research Center, Marshall Space Flight Center, and Armstrong Flight Research Center. Further details about the FOSS system as well as the analysis of flight data can be found in Ref. 5.

This paper discusses the instrumentation selected for LOFTID, a summary of sensor in-flight performance, and will provide examples of data products from the post-flight analysis effort. The naming convention for the LOFTID instrumentation is shown in Table 1. For example:

- H01 as shown in Fig. 2c is the 01 location on the aeroshell.
- LTH01-1 is a TC at the 01 location on the aeroshell (i.e., on the rigid nose) within the FTPS at the 1 location.
- LTH70-R is the radiometer at the 70 location on the aeroshell (i.e., on the center of the rigid nose).
- LPH70-U is the PT at the 70 location on the aeroshell.
- LSF01-Q is the loadcell pin at the 01 location in the forward segment.

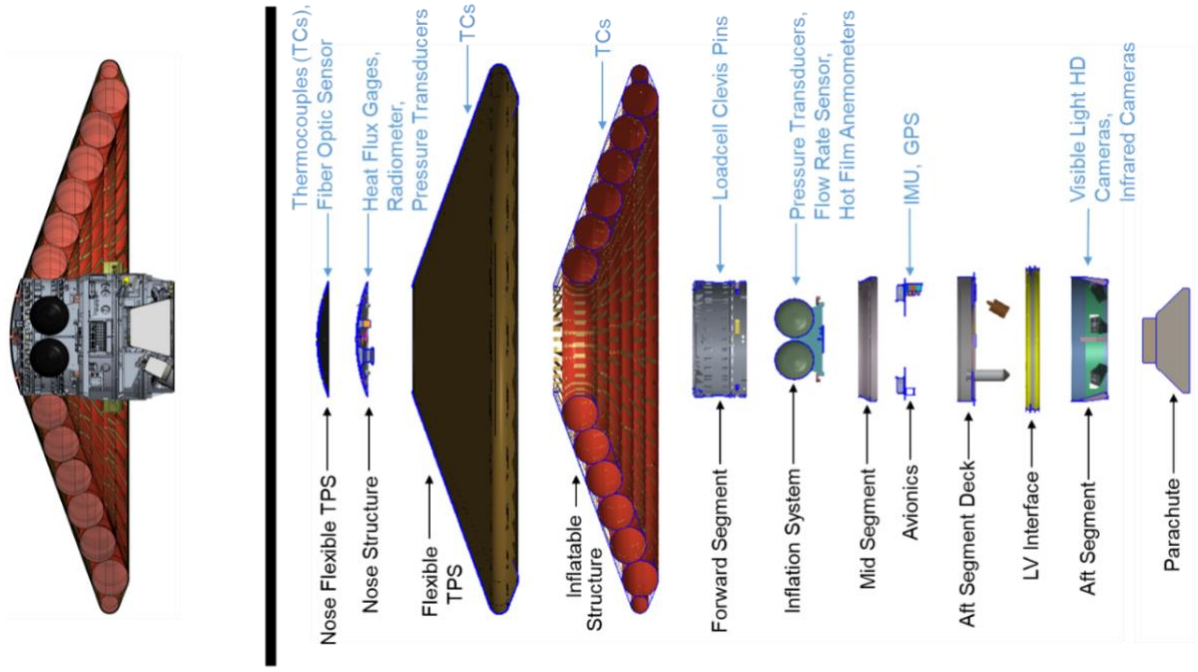

Fig. 1 Cross-section of the LOFTID reentry vehicle and breakdown of the LOFTID instrumentation suite (blue) by location on the vehicle (black).

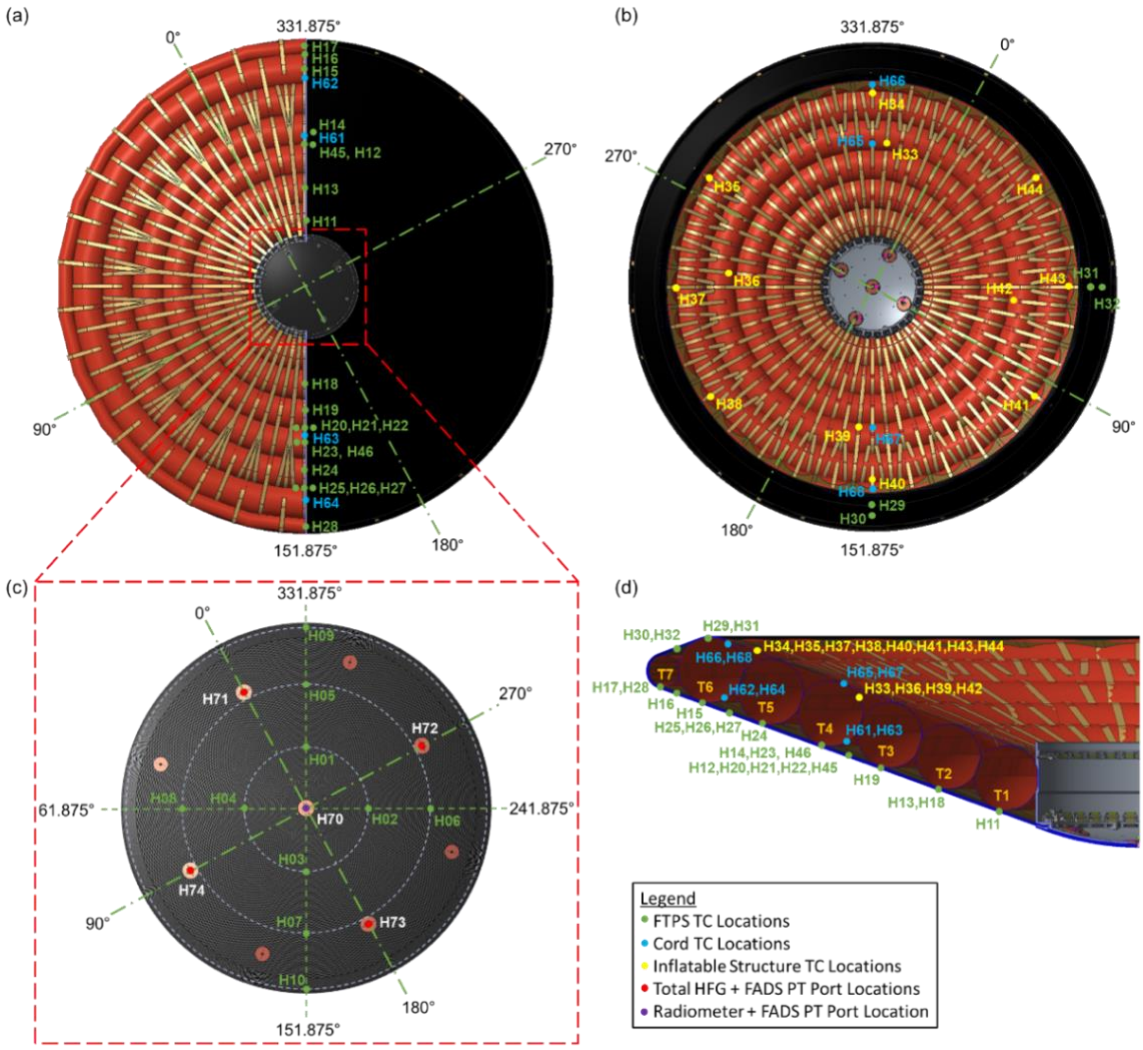

Fig. 2 TC, HFG, and FADS PT port locations on the LOFTID vehicle (a) forebody, (b) aftbody, (c) rigid nose, and (d) cross-section.

Table 1 LOFTID instrumentation naming convention

	Character	Options	Meaning
	1	L	LOFTID
Science Goal	2	P	Pressure
		T	Thermal
		S	Structural
Location	3	H	HIAD Aeroshell
		A	Aft Segment
		F	Forward Segment
	4 & 5	##	Measurement Location ID
	6	-	Dash
Measurement Type	7	#	TC Location
		G	THFG
		Q	Loadcell
		R	Radiometer
		U	Pressure Transducer

III. Thermocouples

The LOFTID instrumentation suite included 82 TCs on the aeroshell to measure the in-depth thermal response: 22 TCs integrated in the FTPS on the rigid nose, 36 TCs in the FTPS on the deployable structure, and 24 TCs on the inflatable structure. LOFTID flew the second generation FTPS with a layup that consisted of two outer layers of silicon carbide (SiC), three insulating layers of Sigratherm KFA-5 carbon felt, one insulating layer of Pyrogel 2250, and one Teflon-Zylon Laminate (TZL) gas barrier layer. TCs were integrated at three different in-depth locations within the FTPS stack as shown in Fig. 3. Fig. 4 shows an example of the routing for the TCs in the FTPS on the rigid nose and the deployable structure. The TCs in the FTPS on the rigid nose were routed from the measurement location through the HFG heat sink to get into the centerbody and connect to the aeroshell data acquisition unit (ADAU). The TCs in the FTPS on the deployable structure were routed within the same layer of the FTPS that they were monitoring the temperature back to the rigid nose and into the ADAU in the vehicle centerbody. This approach eliminated the need to open holes in the FTPS layers to allow the TCs to travel through-the-thickness to the desired FTPS layer which could provide a "thermal short" allowing the external environment to bypass the FTPS insulators at instrumentation locations.

Pre-flight measurement uncertainty reduction testing found major issues with the heritage TCs (30 AWG Type K TCs with a glass braid insulation) that were baselined for use within the LOFTID FTPS [6, 7]. At LOFTID-relevant test conditions, conductive deposits on the glass braid insulation were shown to electrically short the TC leads, the glass insulation melted, and the Type K TCs experienced green-rot (oxidation of the Chromel leg). All of these issues resulted in large measurement errors which could be difficult to identify and quantify in the flight data. Mitigation strategies were developed to minimize the known error sources. Namely, a mica tape wrap was used on each individual TC lead as a barrier to prevent conductive deposits from electrically shorting the TC leads, ceramic insulation was used instead of glass insulation, and Type N TCs which are less susceptible to green-rot were used in place of Type K TCs. The TC and insulation type used in each layer of the FTPS are listed in Table 2. The Type N and Type K TCs were special orders from Pelican Wire. The Type R TC wire, which measured the highest temperatures on the vehicle (-1 location in the FTPS on the rigid nose), was ordered from Pelican and the leads were flame sprayed by Modern Machine and Tool with alumina to insulate them from the surrounding TPS material.

A snapshot of the LOFTID flight TC data is shown in Fig. 5. The LOFTID flight TCs provided a rich data set, although about 5% of the TCs still exhibited electrical shorting behavior. Ways to further mitigate TC electrical shorting issues will be investigated for future HIAD missions. A deep dive into all the LOFTID flight TC data including discussion of the measurement anomalies is presented in Ref. 8. Additionally, the LOFTID flight TC data is being used for thermal model correlation/refinement and inverse analysis to determine surface heating [9].

The uncertainty in the Type N and Type K TC measurements includes the special limits of error wire calibration per ASTM E230 [10], metal composition changes due to interaction between the TC wire and insulation, and ADAU measurement uncertainty. The uncertainty in the Type R TC measurements includes the same error sources as the Type N and Type K TCs with the addition of extension wire error. The measurement uncertainty at 95% confidence level was estimated to be ±1.6% for the Type N and Type K TCs and ±1.3% for the Type R TCs.

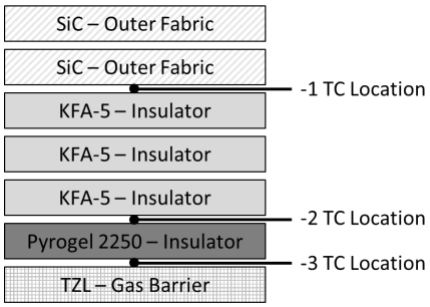

Fig. 3 LOFTID FTPS stack and TC locations.

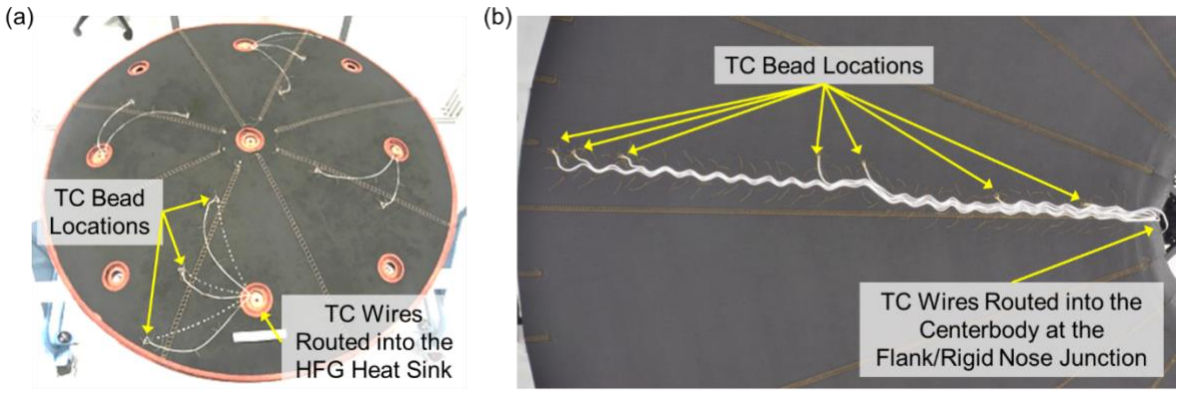

Fig. 4 TC routing on the (a) rigid nose and (b) flank FTPS.

Table 2 LOFTID TC and insulation types

FTPS Location	TC Type	TC Insulation
Nose, -1	Type R	Flame Spray Alumina
Nose, -2	Type N	Mica/Ceramic
Nose, -3	Type K	Mica/Glass
Flank, -1	Type N	Mica/Ceramic
Flank, -2	Type K	Mica/Glass
Flank, -3	Type K	Mica/Glass

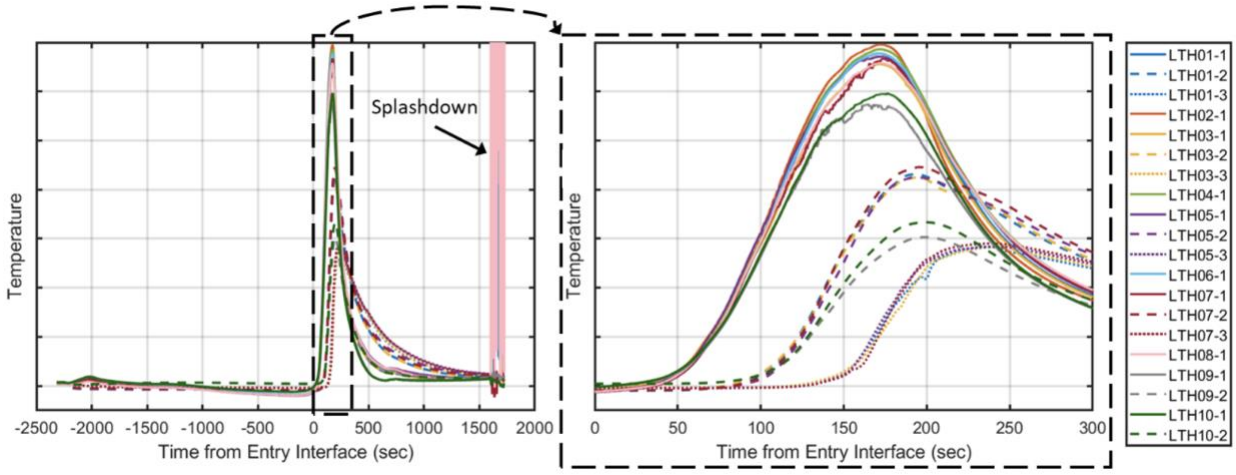

Fig. 5 LOFTID rigid nose flight TC data.

IV. Heat Flux Gages

There were four THFGs and one radiometer flush mounted on the LOFTID rigid nose. The LOFTID THFGs (MEDTHERM model 64-62SB-96-22020KS), shown in Fig. 6a, utilize a Schmidt-Boelter gauge with a high emissivity coating to measure combined convective and absorbed radiative heating, that is:

$$q_{THFS} = q_{convective} + \alpha q_{radiative} \tag{1}$$

where α is the Schmidt-Boelter gauge coating absorptance. The THFGs have a measurement range of 0 - 70 W/cm^2 and include a surface Type K TC embedded in the epoxy surrounding the Schmidt-Boelter gauge. The THFGs were calibrated using NASA Ames' Quartz Lamp Bank (QLB) facility. The calibrations were performed by applying five different heat fluxes (spanning the sensor's measurement range) to a calibrated reference sensor and a LOFTID THFG. The calibration coefficients were determined by applying a least-squares fit of the form

$$q = cV_{THFS} \tag{2}$$

where q is the reference sensor heat flux in W/cm^2, c is the calibration coefficient in W/cm^2 per mV, and V_{THFS} is the LOFTID THFG output in mV. The calibration includes a correction for the pristine coating absorptance of 92%. An approximate correction factor was applied to account for the temperature dependence of the sensor's output [38]. Including this correction factor, Eq. 2 becomes

$$q = c\left(\frac{a_1 T_{cal} + a_0}{a_1 T_{use} + a_0}\right) V_{THFS} \tag{3}$$

where a_0 and a_1 are the temperature dependent correction coefficients, T_{cal} is the temperature of the sensor during calibration, and T_{use} is the temperature of the sensor during use. Further details about this correction factor can be found in Ref. [38].

The LOFTID radiometer (MEDTHERM model 64-3SB-96-22186), shown in Fig. 6b, is a specialized version of the THFG that includes a sapphire window over the Schmidt-Boelter gauge. The sapphire window blocks convective heating, enabling the measurement of radiative heating through its view factor. The radiometer has a measurement range of 0 - 3 W/cm^2 and includes a surface Type K TC embedded in the epoxy surrounding the Schmidt-Boelter gauge. The calibration was performed by MEDTHERM and reported as a least-squares fit per Eq. 2. The manufacturer reported view factor of 0.829 is based upon the geometric dimensions of the radiometer, given the angles shown in Fig. 6b. This view factor does not include refraction from the sapphire window which turn the incident rays toward the normal direction thus increasing the view factor [12]. The view factor correction has not been accounted for yet and is left as future work.

The uncertainty in the THFG and radiometer measurements includes calibration uncertainty, ADAU measurement uncertainty, and sensor temperature dependence. The uncertainty in the surface TC measurement is estimated to be ±3.9°C at 95% confidence and includes the wire calibration error per ASTM E230 [10], extension wire and connector errors, and ADAU measurement uncertainty. The uncertainty in the surface TC measurement is included in the sensor temperature dependence uncertainty. The random uncertainties are combined using the root sum square method and expanded to a 95% confidence level. At peak heating, the uncertainty in the THFG and radiometer measurements are estimated as ±5.1% and ±3.4%, respectively.

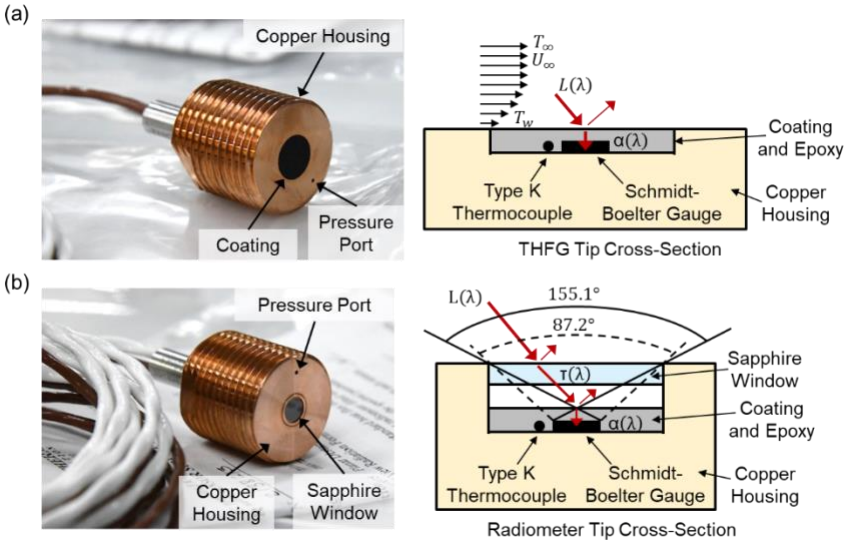

Fig. 6 LOFTID (a) THFG and (b) radiometer.

The flight data from the LOFTID THFGs and radiometer is shown in Fig. 7. Prior to atmospheric entry, all sensors had an increase in signal between the packing restraint release and the turn to separation attitude which aligns with solar radiation. The vehicle rotation can be seen in the data after the start of spin-up and the magnitude of the oscillations align with Earth's radiation. The measured heat flux during entry is not a smooth curve which could be attributable to the way the sensors were mounted in the rigid nose. The large copper sensor housing and heat sink are

flat and possibly sit slightly recessed or proud of the surrounding FTPS. Additionally, there is a ring of RTV between the heat sink and FTPS to prevent flow through into the centerbody, but the surface of the RTV burned off during entry. Both the flushness of the sensor surface to the surrounding FTPS, and then RTV decomposition could directly affect the aerothermal environment experienced by the THFGs. Lastly, the THFG at the LTH74 location measured lower heating prior to peak heating than the other three THFGs. The reason for this is still under investigation. A detailed analysis of the aerothermal environment including comparison of the THFG data to predictions is included in Ref. 13.

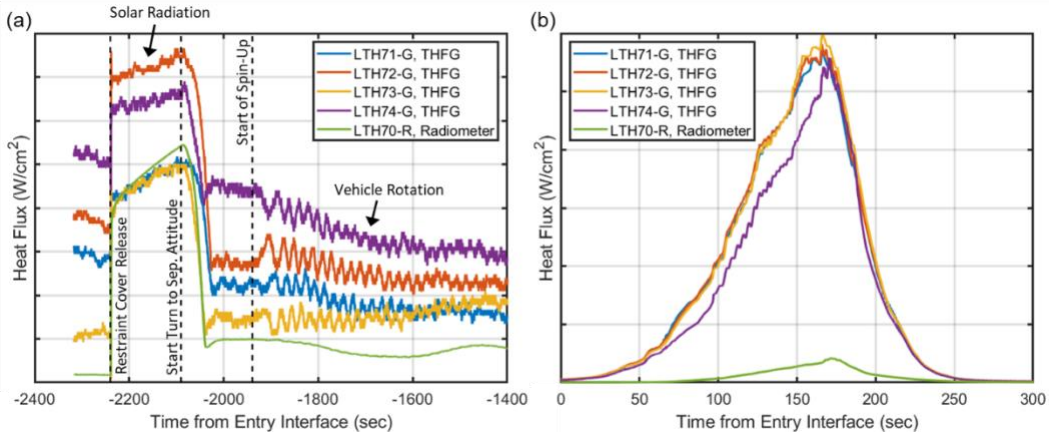

Fig. 7 LOFTID THFG and radiometer flight data (a) prior to atmospheric entry and (b) during entry.

V. FADS Pressure Transducers

There were five PTs measuring the surface pressure distribution on the rigid nose. The LOFTID PTs were GE UNIK 5000 (part number: PMP5023-TB-A3-CC-H0-PE), as shown in Fig. 8a, and had a measurement range of 0 – 1.5 psia. A TC was bonded near the sensing element to enable thermal correction of the data. A full thermal calibration was completed prior to integration into the rigid nose. The PTs were mounted on the backside of the THFG and radiometer heat sinks and connected to the pressure ports in the THFGs and radiometer via flexible tubing. The uncertainty in the PT measurements includes the combined effects of non-linearity, hysteresis, and repeatability across all temperatures, vibration sensitivity, long term stability, and ADAU measurement uncertainty. At 1.5 psia, the measurement uncertainty was estimated to be ±0.3% at 95% confidence level. The flight data from the LOFTID PTs is shown in Fig. 8b. This data became even more crucial for flight reconstruction after the realization that the IMU data was not recorded, allowing for angle of attack determination and structural load estimates. The LOFTID flight mechanics and trajectory reconstruction which uses the FADS PT data is detailed in Ref. 14 and 15.

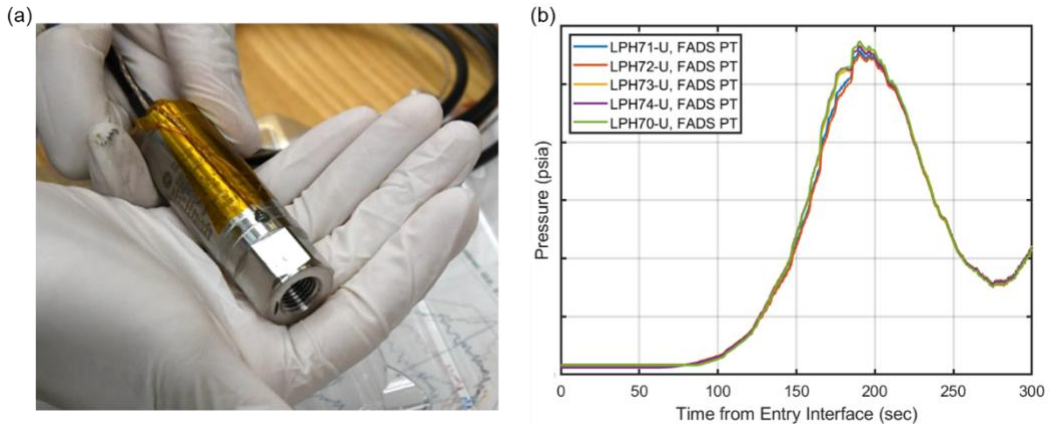

Fig. 8 (a) LOFTID FADS PT with TC bonded near the sensing element and (b) flight data.

VI. Loadcell Pins

The LOFTID instrumentation suite included 12 loadcell pins to measure the total load reacted at each cardinal position (0°, 90°, 180°, and 270°). As shown in Fig. 9b, there were three loadcell pins at each position: (1) the innermost torus forward strap, (2) the innermost torus aft strap, and (3) the radial strap that shunts load from the outer inflatable structure to the rigid centerbody. The loadcell pins were manufactured by Novatech (model: F312-Z5022) and had a range of 0-2500 lbf. The final calibration of the flight loadcell pins was conducted using an MTS Insight load frame, flight-like clevises, and the flight ADAU. The uncertainty in the loadcell pin measurements includes non-linearity, repeatability, thermal effects, clevis manufacturing tolerances, and ADAU measurement uncertainty. At the peak flight load, the measurement uncertainty was estimated to be ±3.0% at 95% confidence level.

The loadcell pin flight data is shown in Fig. 10. The data was corrected for the in-flight zero load which was taken after the packing restraint was released and before tori inflation began. In addition to measuring the strap loads, the loadcell pin data has been used to correlate many entry events. Prior to entry, the load was not evenly distributed across the aeroshell, in particular, the 90° aft (LSF06-Q) strap was carrying the majority of the load. At ~96 sec after entry interface, there is a distinct jump in the loadcell pin data caused by the aeroshell re-seating itself on the centerbody as entry loading was beginning. The aeroshell re-seat is also seen in the camera pod videos and is discussed in more detail in Section VI. At ~185 sec after entry interface, there is a discontinuity in the loadcell pin data which is hypothesized to be due to a low-density region in the atmosphere. The loadcell pin data levels off when the vehicle is in the low-density region and then the a sudden increase in the data occurs when the vehicle exits the low-density region. Lastly, parachute deployment and splashdown are seen in the loadcell pin data at ~650 sec and ~1600 sec after entry interface, respectively. The loadcell pin data indicates that the structural response of the vehicle during flight matches pre-flight predictions and the response seen in ground-based static load testing [3]. Finally, there is an on-going effort which uses the loadcell pin data to correlate and refine structural models for future HIAD applications.

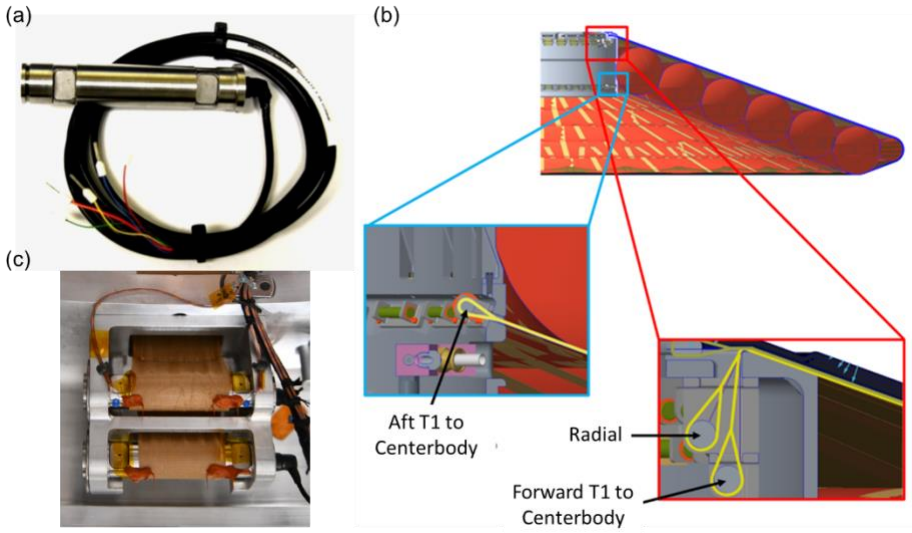

Fig. 9 (a) LOFTID loadcell pin, (b) cross-section of the LOFTID vehicle showing the location of the loadcell pins to measure the aft, forward, and radial straps, and (c) forward and radial loadcell pins installed on the LOFTID vehicle.

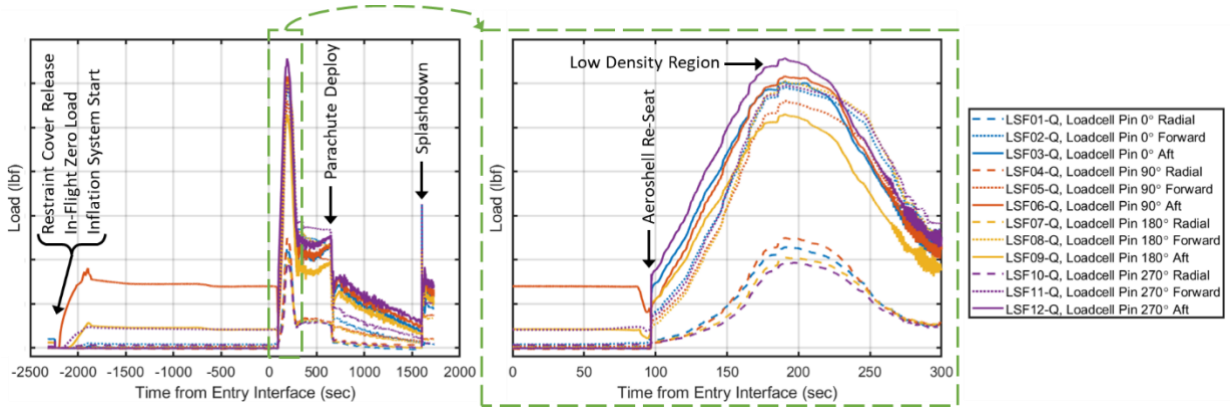

Fig. 10 LOFTID loadcell pin flight data.

VII. Cameras

A. Visible Light and IR Camera Pods

There were six camera pods mounted on the aft segment as shown in Fig. 11. Each camera pod contained one visible light HD camera, two infrared cameras, and an LED light ring. The camera pods provided 360° video of the aft-side of the aeroshell, as shown in Fig. 12, from deployment through splashdown. The camera pod video enabled structural deflection monitoring and measurements of the surface temperature distribution. It is worth noting that one of the six visible light camera pod cameras was not functional during flight due to a known intermittent issue discovered in vibration testing, but all other cameras worked as planned.

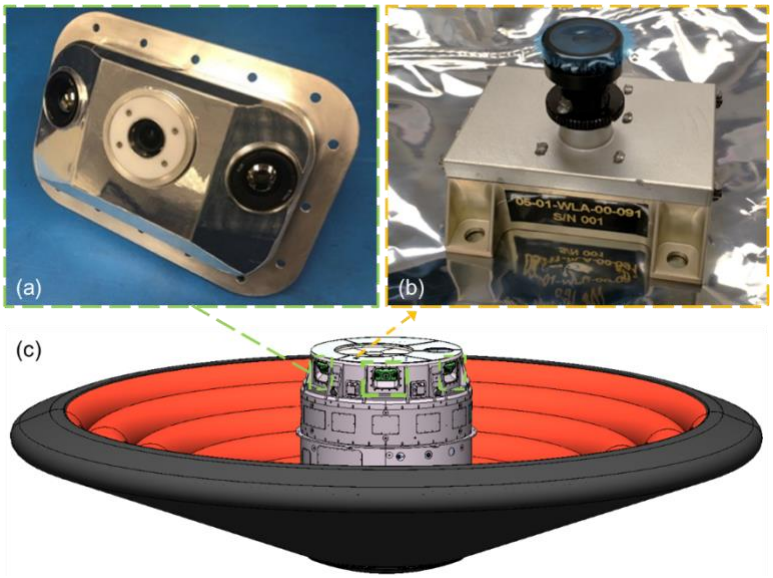

Fig. 11 LOFTID (a) camera pod with one visual and two infrared camera, (b) uplook camera, and (c) location of the camera pods and uplook camera on the LOFTID vehicle.

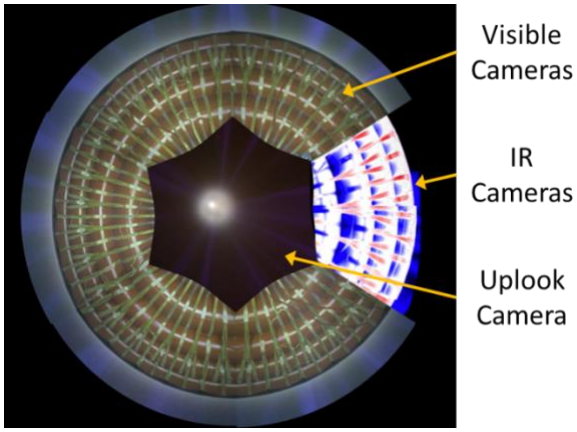

Fig. 12 Example of all camera views stitched together to give 360° coverage of the aft-side of the aeroshell.

To estimate the deflection of the aeroshell during entry, a computer vision algorithm was designed using the *OpenCV* package in Python, which allows the user to select a feature and track its coordinates throughout a video. A Discriminative Correlation Filter with Channel and Spatial Reliability tracker (CSRT) [16] was chosen due to its better accuracy and robustness when compared with the other tracker types built into *OpenCV*. The algorithm's output was the coordinates (in pixels) of the feature throughout the video. The aeroshell deflection angle calculation, further detailed in Ref. 17, required the magnitude of the shift in pixels in the y-direction of the tracked feature and the distance of the feature from the camera location. In this case, unique TC wire run features were chosen for tracking, due to their continued visibility even during periods where the rest of the aeroshell was obscured by plasma; an example is shown in Fig. 13.

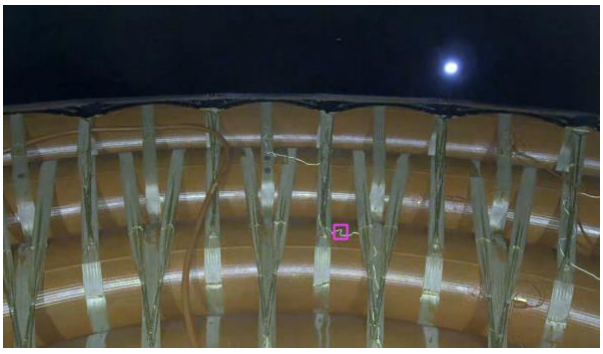

Fig. 13 Frame from visible camera with pink box drawn around TC feature being tracked.

Deflection angles were calculated relative to the configuration of the aeroshell at the end of the video (after the pressure pulse) because a significant jump in aeroshell configuration was observed shortly before the start of the pressure pulse. This movement is likely related to the innermost torus shifting into a mating groove in the vehicle centerbody once a non-negligible pressure force had been applied. The angle of deflection between final aeroshell configuration and peak pressure was 1.3-1.5° (Fig. 14). The configuration of the aeroshell at the end of the pressure pulse likely corresponds to a deflection of 0.5°, based on the expected hysteresis and the deflection measured observed during static load testing at low load after peak loading.

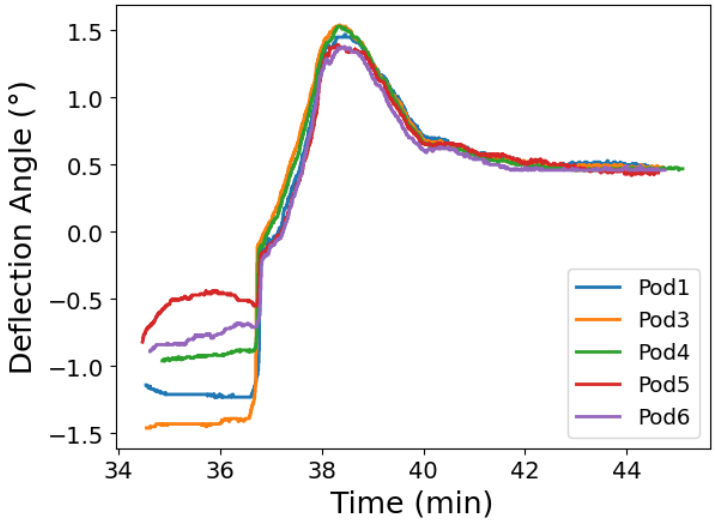

Fig. 14 Deflection angles calculated for each camera pod location throughout the duration of the pressure pulse.

B. Uplook Camera

There was one uplook camera mounted on the aft segment as shown in Fig. 11. The uplook camera procured from Deep Space Systems was a modified GoPro Hero 4 Black and included an embedded microphone. The video recorded by the uplook camera was stored on an internal micro-SD card. The uplook camera was primarily intended to capture separation from the Centaur and parachute dynamics. Still images from the uplook camera video during each of these events are shown in Fig. 15a and Fig. 15c. The video from these events indicates that separation from the Centaur went nominally and that the parachute deployment and subsequent dynamics were benign.

Fig. 15 Images from the uplook camera video during (a) separation, (b) atmospheric entry, and (c) parachute deployment.

The video of the vehicle wake (Fig. 15b) and recompression shock during atmospheric entry has also been valuable for characterizing entry science and vehicle performance. Once the LOFTID vehicle began to see sensible heating, a fascinating evolution in the structure, color, size, and dynamics of the vehicle wake unfolded. Computer vision techniques were applied to this video to quantify the relative position of the central recompression shock as a function of time. Fig. 16 presents the results from this analysis and shows that the recompression shock position reflected the angle of attack bias and oscillations during entry that are observed in the FADS data [15]. This analysis technique has also been leveraged to show that the ~2m diameter of the recompression shock near peak heating is consistent with pre-flight predictions using CFD. Fig. 17 shows the diversity of wake structures and color spectra that were captured. This video could support future analysis on the dynamics and characterization of the wake flow aerothermal environments. Finally, the camera was fortunate to capture the full moon in its field of view for the final descent portion of the trajectory prior-to and after parachute deployment. The dynamics of the moon in this field of view provide an opportunity for future work to extract quantitative vehicle dynamics to compensate for the lack of available IMU data.

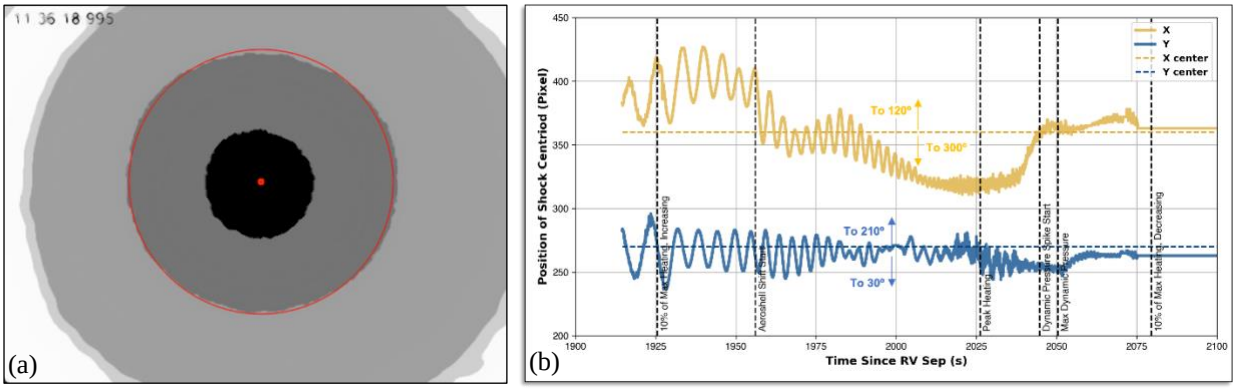

Fig. 16 (a) Modified frame from the uplook camera showing the identified perimeter and centroid of the recompression shock and (b) lateral (X) and vertical (Y) position of the shock centroid as a function of time since separation from the Centaur.

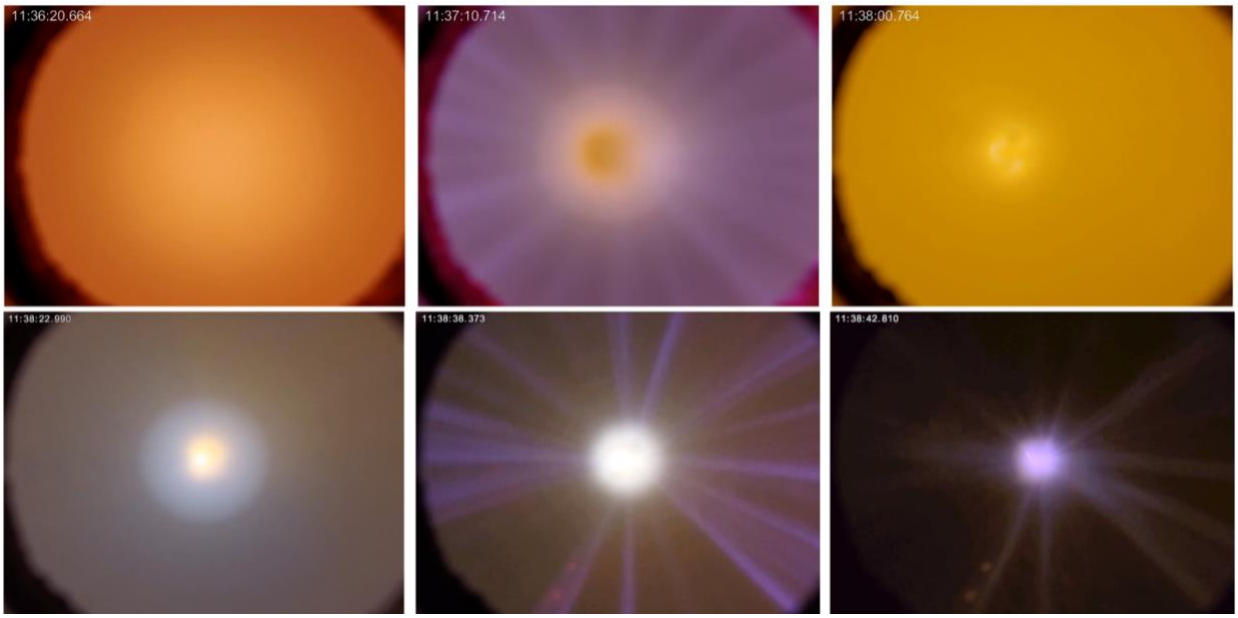

Fig. 17 Snapshots from the uplook camera at progressive points in time throughout the sensible heating portion of the entry trajectory show a variety of wake structure and visual spectrum content.

Fig. 18 shows the spectrograms of the uplook camera audio from the time the uplook camera was turned on (~15 seconds prior to LOFTID being released from the Centaur) through splashdown. Key events identified in the spectrograms include release from the Centaur, ejection of the ejectable data recorder (EDR), parachute mortar fire, and splash down. The opening of the inflation system relief valves can also be seen in the spectrograms and is an important data point to support the analysis of the inflation system performance as detailed in Ref. 4.

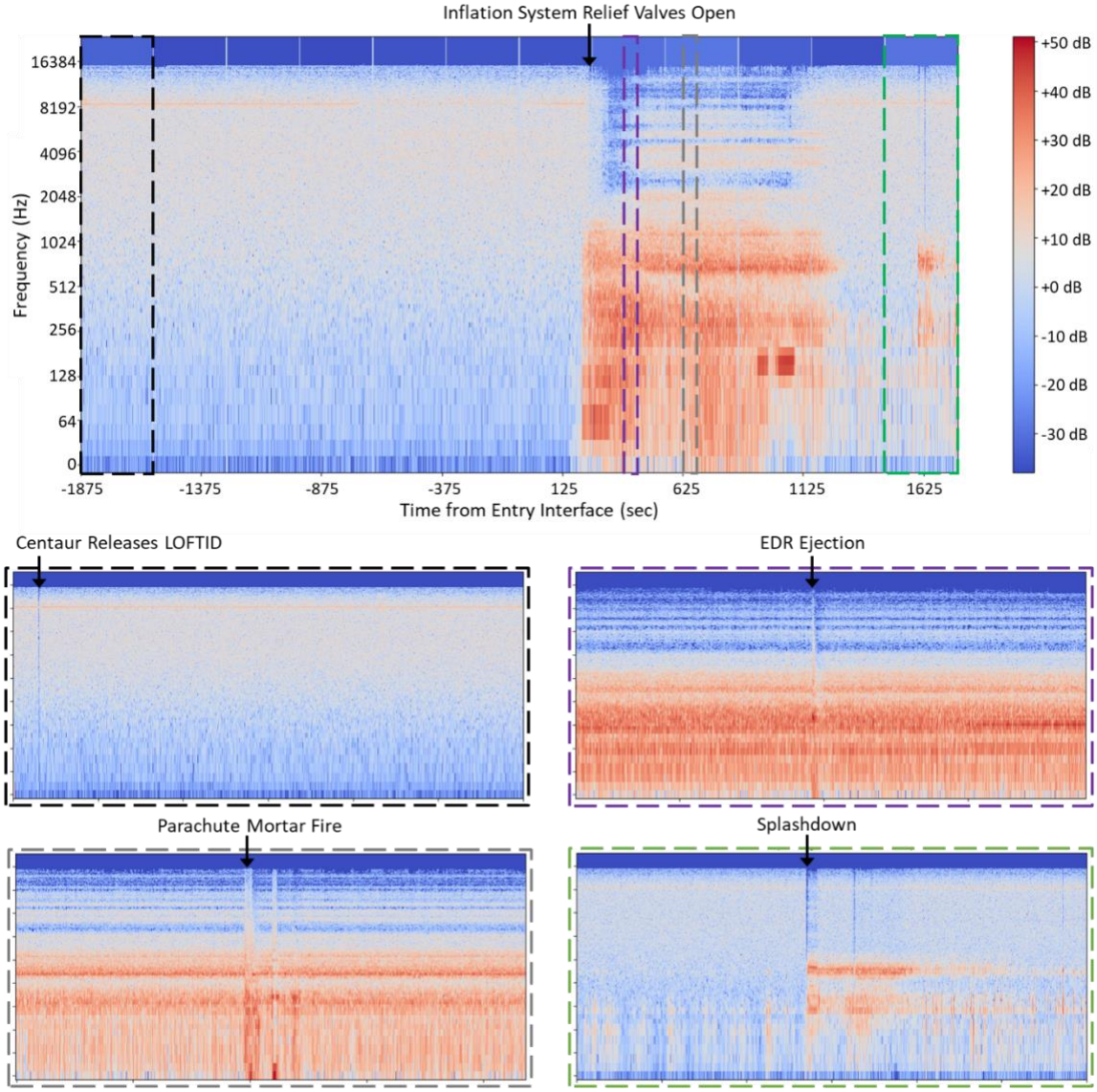

Fig. 18 Spectrogram for the uplook camera audio with key events identified.

VIII. Conclusion

The LOFTID instrumentation performed as expected and generated an incredibly rich dataset including temperatures, heat rates, pressures, loads, and video totaling over 150 science measurements. This data is allowing HIAD analytical model validation across multiple disciplines and laying the path to scale up the technology for future applications [4, 9, 13]. With the loss of the IMU data, many of the remaining datasets were creatively employed beyond their originally planned use to complete trajectory reconstruction [14, 15]. In addition to the analog sensors, the entirety of the camera suite proved to be invaluable not only for the direct science it enabled, but in providing contextual information for all the other system measurements to aid in their interpretation. Future applications using the HIAD technology plan to incorporate a similar instrumentation suite in order to continue further development and validation of the technology's analytical tools, working toward system designs that can enable large scale missions such as humans to Mars.

Acknowledgments

The authors would like to thank Ben Libben and Chris Naughton for their work in support of the aeroshell instrumentation. Joseph Williams is supported through contract NNA15BB15C to AMA, Inc.

References

[1] Cheatwood F.M., et al., "Manufacturing Challenges and Benefits when Scaling the HIAD Stacked-Torus Aeroshell to a 15m-Class System" IEEE Aerospace Conference, 2016
doi: 10.1109/AERO.2016.7500773

[2] DiNonno, J., and Cheatwood, N., "Low-Earth Orbit Flight Test of an Inflatable Decelerator (LOFTID) Mission Overview and Science Return," paper submitted to AIAA SciTech 2024, Orlando.

[3] Hughes, S.J., Swanson, G., Cheatwood, N., and DiNonno, J., "Low-Earth Orbit Flight Test of an Inflatable Decelerator (LOFTID) Aeroshell Performance," paper submitted to AIAA SciTech 2024, Orlando.

[4] Blakeley, H.S., Bodkin, R.J., and Emmett, A., "Heritage to Flight; The Test Program that Brought an Inflation System Back to Life," paper submitted to AIAA SciTech 2024, Orlando.

[5] Parker, A.R., et al., "Fiber Optics Sensing System (FOSS) deployment on Low-Earth Orbit Flight Test of an Inflatable Decelerator (LOFTID)," paper submitted to AIAA SciTech 2024, Orlando.

[6] Miller, R.A., Kazemba, C.D., Swanson, G.T., and Williams, J.D., "Electrical Shorting of Thermocouples in Flexible Thermal Protection System Materials," *AIAA JSR*, Vol. 60, No. 2, 2023, pp. 591-600.
doi: 10.2514/1.A35500

[7] Miller, R.A., Kazemba, C.D., Swanson, G.T., Williams, J.D., Hughes, S., and Cheatwood, N., "Arcjet Evaluation of Thermocouple Performance in Flexible Thermal Protection System Materials," *AIAA JSR*, Vol. 60, No. 4, 2023, pp. 1043-1354.
doi: 10.2514/1.A35595

[8] Miller, R.A., Swanson, G., Kazemba, C., Alpert, H., and Williams, J., "Evaluation of the LOFTID Flight Thermocouple Measurements," paper submitted to AIAA SciTech 2024, Orlando.

[9] Tobin, S.A., Brune, A.J., and Bowes, A., "LOFTID Aeroshell Thermal Response Uncertainty Analysis utilizing the End-to-End Monte Carlo Approach," paper submitted to AIAA SciTech 2024, Orlando.

[10] ASTM E230/E230M – 17, "Standard Specification for Temperature-Electromotive Force (emf) Tables for Standardized Thermocouples."

[11] Miller, R.A., and Alpert, H.A., "Temperature dependent performance of Schmidt-Boelter heat flux sensors," *Review of Scientific Instruments*, Vol. 94, 025002, 2023.
doi: 10.1063/5.0129703

[12] Scoggins, J.B., Mazaheri, A., and Johnston, C.O., "Development of an Optical Model for the MEDLI2 Radiometer," AIAA 2023-4037.
doi: 10.2514/6.2023-4037

[13] Hollis, B.R., Wise, A.J., Liechty, D.S., Korzun, A.M., and Thompson, K.B., "Aerothermodynamics Analyses for the LOFTID Technology Demonstration Mission," paper submitted to AIAA SciTech 2024, Orlando.

[14] Deshmukh, R., Dutta, S., Bowes, A., and DiNonno, J., "Flight Mechanics Analysis of Low-Earth Orbit Flight Test of an Inflatable Decelerator," paper submitted to AIAA SciTech 2024, Orlando.

[15] Karlgaard, C.D., Deshmukh, R., Dutta, S., Korzun, A.M., and Hollis, B.R., "Trajectory Reconstruction of the Low-Earth Orbit Flight Test of an Inflatable Decelerator," paper submitted to AIAA SciTech 2024, Orlando.

[16] Lukezic, A., Vojir, T., Zajc, L.C., Matas, J., and Kristan, M., "Discriminative Correlation Filter with Channel and Spatial Reliability," CVPR, 2017, pp. 6309-6318.

[17] Alpert, H.S., Kazemba, C.D., and Swanson, G., "Post-Flight Quantification of LOFTID Aeroshell Deflection Using Feature Tracking," IPPW, 2023.